Supporting Information

Enhanced Nonlinear Optical Response of Rectangular MoS$_2$ and MoS$_2$/TiO$_2$ in Dispersion and Film

Xiaohong Li, [†] Kunhong Hu, [‡] Bosai Lyu, [†] Jingdi Zhang, [†] Yingwei Wang, [†] Peng Wang, [†] Si Xiao, [*,†] Yongli Gao, [†,§] and Jun He[*,†]

[†] *Institute of Super-microstructure and Ultrafast Process in Advanced Materials, School of Physics and Electronics, Central South University, 932 South Lushan Road, Changsha, Hunan 410083, P. R. China.*

[‡] *Department of Chemical and Materials Engineering, Hefei University, Hefei 230601, P. R. China.*

[§] *Department of Physics and Astronomy, University of Rochester, Rochester, New York 14627, United States.*

*Corresponding author email:
    sixiao@csu.edu.cn   (S. Xiao), Telephone: +86-18673123070
    junhe@csu.edu.cn   (J. He), Telephone: +86-15802661974

1. The characters of MoS$_2$/TiO$_2$ composite.

The thickness of the samples were mainly characterized by the Atomic force microscopy (AFM). The average thickness of 18 nm for rectangular MoS$_2$ has been shown in manuscript, and the samples are uniform. While the thickness of MoS$_2$/TiO$_2$ composite is really not uniform, as shown in Figure 1. Figure 1(a) is the AFM image of MoS$_2$/TiO$_2$ composite. Figure 1(b) is the height curve of the corresponding line in (a). Figure 1(c) illustrate the histogram of thickness of MoS$_2$/TiO$_2$ composite. More than 64.7% of the nanosheets out of the 56 objects have an averaged thickness between 38 nm and 41 nm.
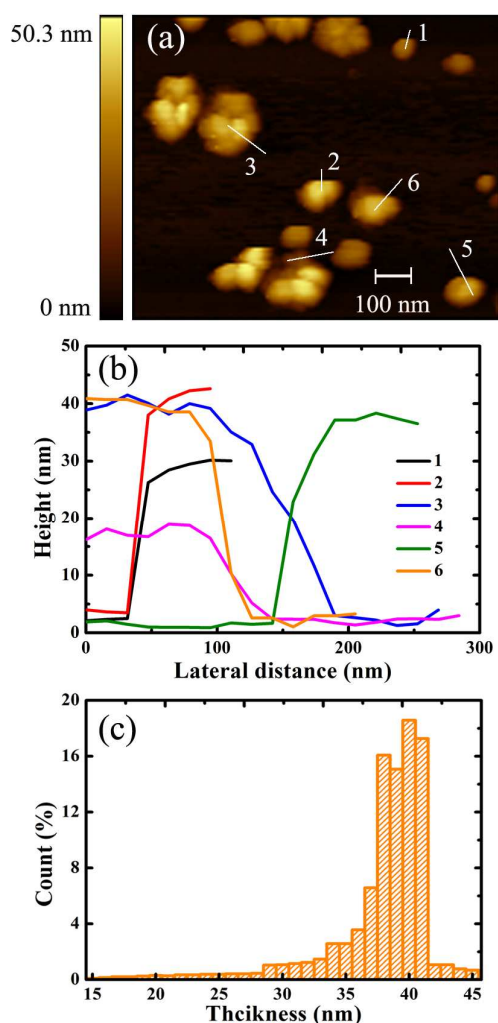
Figure 1. (a) The AFM image of MoS_2/TiO_2 composite. (b) The height curve of the corresponding line in (a). (c) The histograms of thickness of MoS_2/TiO_2 composite.

2. The forming mechanism of SSPM

In the dispersion, each nanoflake is a domain. Each domain oriented arbitrarily, and the wave function of each electron in every domain are out of phase initially. Due to energy relaxation, the photoinduced quasiparticles in each domain have interaction with the electric field of light and assumes its local phase. As the same time, opposite charged carriers travel in opposite direction in the external field and build up the electric polarization. The electric polarization of each domain interacts with the external field, and the rotation torque reorients the domain. In the end, each rectangular domain contains a long-axis parallel to the polarization of external field, as if there are numerous of parallel lines on the polarization of laser, and each rectangular domain is "hung" by a "thread". This is the formation process of the "wind-chime" model. Once the wind chime is formed, the nonlocal electron coherence is set up among each rectangular domain. When the laser passes through the aligned nanoflakes, upon the nonlocal electron coherence enhancement, the coherence SSPM happens in the dispersion and diffraction pattern is received[1]. For MoS_2 and MoS_2/TiO_2 dispersions, both the number and the radius of diffraction rings increase and reach their maximums at 0.95 s and 1.02 s after the beginning of the dynamic SSPM processes.

3. The forming time explanation based on "wing-chime" model

Referring to 1, the time need for the pattern formation is

$$\tau = N_0 \cdot T = \frac{\varepsilon_r \pi \eta \xi R c}{1.72(\varepsilon_r - 1)Ih}.$$

We have assigned the values ε_r = 3.33, R = 80 nm, and h = 18 nm for MoS$_2$, η = 5.5 × 10^{-4} Pa·s for THF, I = 18 GW/cm^2, τ = 0.99 s in this experiment. Then, the parameter ξ =0.1 could be estimated, which is the portion of the fluid globe that is rotating together with the nanoflakes. The parameter ξ is much bigger than that in reference 1. It may be effected by the difference shapes of rectangular and disk, the increasing of constant viscosity coefficient, or the intensity of I at a certain range[1].

4. The theoretical calculation of optical nonlinear refractive index in SSPM.

According to the optical Kerr effect, the intensity dependent effective refractive index of dispersions can be expressed as $n_e = n_{0e} + In_{2e}$, where n_{0e} and n_{2e} are the effective linear and nonlinear refractive index, respectively[2]. And the n_{0e} of dispersion can be calculated with the Bruggeman effective medium theory[3-5]. The solutes' (MoS$_2$ or MoS$_2$/TiO$_2$) influence on linear refractive indexes of dispersions is negligible, so the linear refractive index of the solvent n_{THF} = 1.405 is approximately equal to the MoS$_2$ and MoS$_2$/TiO$_2$ solution dispersions. The phase shift which changes to the incident intensity can be expressed as[6,7]

$$\Delta \psi(r) = \left(\frac{2\pi n_{0e}}{\lambda} \right) \int_0^{L_{eff}} n_{2e} I(r,z) dz \qquad (1)$$

Where λ is the laser wavelength, L_{eff} is the effective optical thickness of the laser beam passing the dispersion, the effective thickness of cuvette can be obtained by[8]

$$L_{eff} = \int_{L_1}^{L_2} \left(1 + \frac{z^2}{z_0^2}\right)^{-1} dz = z_0 \arctan\left(\frac{z}{z_0}\right)\Big|_{L_1}^{L_2} \tag{2}$$

r is the radial position, $I(r, z)$ is the intensity distribution. For a Gaussian beam, the intensity $I(0, z)$ at the center is twice of the average intensity I measured in the experiments. The optical detector shall receive the bright or black ring when the laser beam through the sample dispersion, and the total number of rings N is determined by $[\Delta\psi(0) - \Delta\psi(\infty)] = 2N\pi$ for a given laser intensity[7]. Figure 3b,c show the diffraction patterns with maximum laser intensity. Thus, after a simple derivation, we have

$$n_{2e} = \left(\frac{\lambda}{2n_{0e}L_{eff}}\right)\frac{N}{I} \tag{3}$$

Thus optical nonlinear refractive index n_{2e} is determined to the parameters λ, n_{0e}, L_{eff} and $\frac{N}{I}$, the n_{2e} will be obtained according to the Figure 3d,e which are about the relation between number rings and incidence intensity. In our experiment, N is approximately proportional to I, which is similar to the previous report[9]. The spot radius of 700 nm is 886.9 μm. The focal length of the lens is 200 mm. The quartz cuvette with a pathlength 10 mm was placed 10.8 mm in front of the focal point. By Eq. (2) we can calculate the nonlinear refractive index of MoS_2 is 3.17×10^{-5} cm^2/W and MoS_2/TiO_2 is 2.66×10^{-5} cm^2/W.

5. The explanation that Z-scan experiment is not fit to be performed in dispersion sometimes.

The nonlinear refraction index can be measured by Z-scan because of self-focusing or self-defocusing properties. However, the intensity of the focus in Z-scan is more than that of SSPM, which will result in self-diffraction. Once the self-diffraction is

formed, the spot will be obviously enlarged. Then, the spot may not be received completely as Figure2. The mechanism of self-diffraction is different from self-focusing or self-defocusing. The intensity distribution of self-diffraction spot is the concentric circles rather than the Gaussian. Hence the nonlinear refraction index based on Z-scan is unreliable because the phenomenon of SSPM may be occur in dispersion. As Figure 2 shows, the SSPM results in enlarged spot, then the spot do not be received completely by detector.
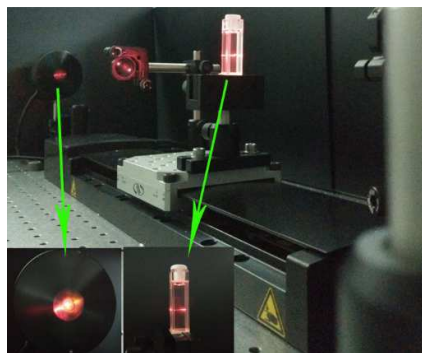

Figure 2. The part setup of Z-scan. The inset is the enlarged image of the detector and cuvette, respectively.

6. The explanation why SSPM is not fit to be performed in films.

On the one hand, the SSPM pattern do not generated in these films. The possible reason is that the nanoflakes is solidified on glass substrate, which can not be reorientated under intensive laser irradiation. The SSPM in 2D material films has not been reported so far. On the other hand, though the self-diffraction of other films (such as solid photopolymerizable organosiloxane) had been reported, thermal effect is the primary mechanism[10]. In this work, the thermal effect can be neglected because of repetition rate (2 kHz) of the fs laser. In addition, thermal effect may result in irreversible damage in film.

7. The explanation for the results of MoS_2 film in OA Z-scan.

With the increasing of intensity, the nonlinear absorption curve about MoS_2 film will change from SA to RSA. It can been explained as that: the electrons in the valence band are easily pumped to fill the conduction band by the high intensity femtosecond pulse, and the optical absorption reaches saturation[11]. Such SA was also observed in many thin film samples, such as GaN[12], $BiMnO_3$[13], $Bi_{3.25}La_{0.75}Ti_3O_{12}$[14], etc. With the increase of the input intensity, the peak of SA for the MoS_2 also increased correspondingly in the OA Z-scan measurements. However, under higher input intensity $I_0 = 9.28$ GW/cm^2 the curve become a typical RSA response, which is similar to the situation reported by reference[4,15]. In order to ensure the incident intensity is under the optical damage threshold, multiple replication measurements are performed. The results are similar, as shown in Figure 3.
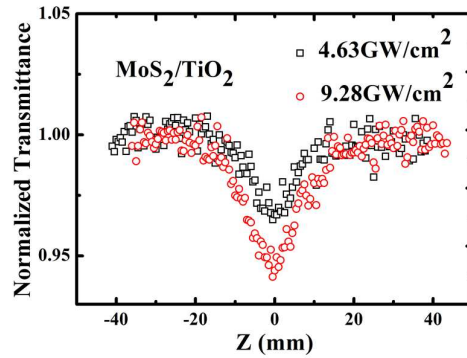

Figure 3. The repetitive opening aperture Z-scan signal for MoS_2/TiO_2 composite.

7. The theoretical calculation of the nonlinear refraction based on Z-scan.

According to the nonlinear optical theory. Based on a spatially and temporally Gaussian pulse, the normalized energy transmittance, $T_{CA}(z)$ is given by[16,17,5]

$$T_{CA} = 1 + \frac{4\Delta\varphi_0 z/z_0}{\left((z/z_0)^2 + 9\right)\left((z/z_0)^2 + 1\right)} \tag{4}$$

Where the phase change $\Delta\varphi_0 = 2\pi n_2 I_0 L_{eff}/\lambda$ I_0. $\lambda = 700$ nm, I_0 is denoted as the peak, on-axis irradiance at the focal point ($z = 0$) within the sample. $I_0 = 4.63$ GW/cm^2, $z_0 = \frac{\pi w_0^2}{\lambda}$. The waist radius $w_0 = 46$ μm, the transmittances of the film samples at 700 nm are 10.43 nj, 12.78 nj and 8.69 nj for MoS$_2$, MoS$_2$/TiO$_2$ and TiO$_2$, respectively.

References

(1) Wu, Y.; Wu, Q.; Sun, F.; Cheng, C.; Meng, S.; Zhao, J. Emergence of Electron Coherence and Two-color All-optical Switching in MoS$_2$ Based on Spatial Self-phase Modulation. *Proc. Natl. Acad. Sci. U.S.A.* **2015**, *112*, 11800-11805.

(2) Wu, R.; Zhang, Y.; Yan, S.; Bian, F.; Wang, W.; Bai, X.; Lu, X.; Zhao, J.; Wang, E. Purely Coherent Nonlinear Optical Response in Solution Dispersions of Graphene Sheets. *Nano Lett.* **2011**, *11*, 5159-5164.

(3) Wang, K.; Feng, Y.; Chang, C.; Zhan, J.; Wang, C.; Zhao, Q.; Coleman, J.; Zhang, L.; Blau, W. J.; Wang, J. Broadband Ultrafast Nonlinear Absorption and Nonlinear Refraction of Layered Molybdenum Dichalcogenide Semiconductors. *Nanoscale* **2014**, *6*, 10530-10535.

(4) Tao, J.; Chai, J.; Guan, L.; Pan, J.; Wang, S. Effect of Interfacial Coupling on Photocatalytic Performance of Large Scale MoS$_2$/TiO$_2$ Hetero-thin Films. *Appl. Phys. Lett*. **2015**, *106*, 081602.

(5) Sheik-Bahae, M.; Said, A. A.; Wei, T.; Hagan, D. J.; Van Stryland, E. W. Sensitive Measurement of Optical Nonlinearities Using a Single Beam. *IEEE J. Quantum*

Electron. **1990**, *26*, 760-769.

(6) Wang, G.; Zhang, S.; Umran, F. A.; Cheng, X.; Dong, N.; Coghlan, D.; Cheng, Y.; Zhang, L.; Blau, W. J.; Wang, J. Tunable Effective Nonlinear Refractive Index of Graphene Dispersions during the Distortion of Spatial Self-phase Modulation. *Appl. Phys. Lett.* **2014**, *104*, 141909.

(7) Wang, G.; Zhang, S.; Zhang, X.; Zhang, L.; Cheng, Y.; Fox, D.; Zhang, H.; Coleman, J. N.; Blau, W. J.; Wang, J. Tunable Nonlinear Refractive Index of Two-dimensional MoS_2, WS_2, and $MoSe_2$ Nanosheet Dispersions [Invited]. *Photon. Res.* **2015**, *3*, A51-A55.

(8) Hu, K.; Hu, X.; Xu, Y.; Sun, J. Synthesis of Nano-MoS_2/TiO_2 Composite and Its Catalytic Degradation Effect on Methyl Orange. *J. Mater. Sci.* **2010**, *45*, 2640-2648.

(9) Shi, B.; Miao, L.; Wang, Q.; Du, J.; Tang, P.; Liu, J.; Zhao, C.; Wen, S. Broadband Ultrafast Spatial Self-phase Modulation for Topological Insulator Bi_2Te_3 Dispersions. *Appl. Phys. Lett*. **2015**, *107*, 151101.

(10) Long, H.; Chen, A.; Yang, G.; Li, Y.; Lu, P. Third-order Optical Nonlinearities in Anatase and Rutile TiO_2 Thin Films. *Thin Solid Films* **2009**, *517*, 5601-5604.

(11) Villafranca, A. B.; Saravanamuttu, K. Diffraction Rings due to Spatial Self-phase Modulation in a Photopolymerizable Medium. *J. Opt. A: Pure Appl. Opt.* **2009**, *11*, 125202.

(12) Huang, Y.; Sun, C.; Liang, J.; Keller, S.; Mack, M. P.; Mishra, U. K. Femtosecond Z-scan Measurement of GaN. *Appl. Phys. Lett*. **1999**, *75*, 3524-3526.

(13) Sharan, A.; An, I.; Chen, C.; Collins, R. W.; Lettieri, J.; Jia, Y.; Schlom, D. G.;

Gopalan, V. Large Optical Nonlinearities in BiMnO$_3$ Thin Films. *Appl. Phys. Lett.* **2003**, *83*, 5169-5171.

(14) Shi, F.; Meng, X.; Wang, G.; Sun, J.; Lin, T.; Ma, J.; Li, Y.; Chu, J. The Third-order Optical Nonlinearity of Bi$_{3.25}$La$_{0.75}$Ti$_3$O$_{12}$ Ferroelectric Thin Film on Quartz. *Thin Solid Films* **2006**, *496*, 333-335.

(15) Loh, K. P.; Zhang, H.; Chen, W.; Ji, W.; Templated Deposition of MoS$_2$ Nanotubules Using Single Source Precursor and Studies of Their Optical Limiting Properties. *J. Phys. Chem. B* **2006**, *110*, 1235-1239.

(16) Shen, Y. *Principles of Nonlinear Optics*; Wiley-Interscience, New York, USA, 1984.

(17) Divya, S.; Nampoori, V. P. N.; Radhakrishnan, P.; Mujeeb, A. Morphology Dependent Dispersion of Third-order Optical Nonlinear Susceptibility in TiO$_2$. *Appl. Phys. A* **2014**, *114*, 1079-1084.